Monolithically Integrated InP-Based Front-End Photoreceivers

Yousef Zebda, Richard Lai, Pallab Bhattacharya, *Fellow, IEEE,* Dimitris Pavlidis, *Senior Member, IEEE,* Paul R. Berger, *Member, IEEE,* and Timothy L. Brock

***Abstract*—The performance characteristics of a monolithically integrated front-end photoreceivers, consisting of a photodiode and a MODFET amplifier, have been analyzed and measured. A vertical scheme of integration was initially used to realize a photoreceiver circuit on InP consisting of a InGaAs p-i-n diode, an InGaAs/InAlAs pseudomorphic MODFET, and passive circuit elements. The device structures were grown by single-step molecular beam expitaxy with an isolating layer in between. The microwave performance of 1-μm gate MODFET's in the circuit is characterized by f_T = 9 GHz, although identical discrete devices have f_T = 30–35 GHz. The degradation is due to additional parasitic capacitances present in this scheme of integration. In spite of this disadvantage the bandwidth of the circuit is 2.1 GHz. Integration of the p-i-n diode with 1.0- and 0.25-μm gate MODFET's has also been done in a planar scheme, using regrowth, and receiver bandwidths of 6.5 GHz are measured. This value is comparable to hybrid circuits with InP-based devices.**

I. Introduction

In the design of an optical fiber communication system, whether for use in long-distance communication or for bussing data over short distances, and operating at low or high data rates, a key element is the receiver. The basic purpose of the receiver is to detect the incident light and convert it into an electrical signal containing the information impressed on the light at the transmitting end. The receiver is thus an optical-to-electrical (O/E) transducer.

The front end of a photoreceiver consists of a photodiode and a single-stage amplifier. The fundamental goal in the design of an optical receiver is to minimize the amount of optical power which must reach the receiver in order to achieve a given bit error rate (BER) in a digital system, or a given signal-to-noise ratio (S/N) in an analog system. This amount of power is referred to as the sensitivity of the receiver.

Design of a receiver can follow one of two approaches. The first is the hybrid approach where different devices are fabricated on different substrates and are packaged separately while assembled in the same circuit. The other is the monolithic approach where the whole receiver circuit is built on the same substrate. In this technique the parasitic capacitance and bonding wire inductance can be minimized, and smaller size and lower cost can be achieved.

There are two basic schemes for fabricating a monolithically integrated photoreceiver. The first is a vertical structure in which the epitaxial layers for the photodetector and the amplifier are sequentially grown on the same substrate with an isolating layer between the two devices. The other scheme is a planar one in which both device structures are formed on the same substrate, either using the same layers, or by using regrowth and two-step epitaxy. In the first structure, although only a single epitaxial growth step is required, a high-quality insulating layer between the two devices is necessary. Also, there is capacitive interference among electrical elements caused by the existence of a highly doped semiconductor under all the active components. The second structure has no capacitive coupling problem, but is limited either by regrowth and the associated interface quality or by the need to use identical layers for both devices.

Monolithically integrated p-i-n photodiodes and field-effect transistors (FET) are very attractive for the design of front-end photoreceivers. Early work in this area, using these devices, has been done with both the GaAs- and InP-based material systems [1]–[7]. Using InP-based materials, Kasahara *et al.* [8], have integrated an InGaAs p-i-n photodiode with an InP metal insulator semiconductor FET (MISFET) grown sequentially by LPE and VPE, and they were able to achieve an impulse response of 100 Mb/s. Matsuda *et al.* [9] have reported the integration of an InGaAs p-i-n photodiode with four junctions FET's (JFET) grown by LPE, and they were able to achieve a 3-dB frequency of 240 MHz. Nobuhara *et al.* [10] have demonstrated an InGaAs/InAlAs modulation-doped FET (MODFET) integrated with an InGaAs p-i-n photodiode with a sensitivity of −23.7 dBm at 2 Gb/s. But the best results by far have been demonstrated by Miyagawa *et al.* [11], who demonstrated a 3-dB frequency of 7 GHz using

Manuscript received May 17, 1990; revised December 10, 1990. This work was partly supported by the Army Research Office (URI Program) under Contract DAAL03-87-K0007 and partly by Boeing Aerospace and Electronics. The review of this paper was arranged by Associate Editor G. Craford.

Y. Zebda was with the Center for High-Frequency Microelectronics and Solid State Electronics Laboratory, Department of Electrical Engineering and Computer Science, The University of Michigan, Ann Arbor, MI 48109-2122. He is now with the Electrical Engineering Department, Jordan University of Science and Technology, P.O. Box 3030, Irbid, Jordan.

R. Lai, P. Bhattacharya, D. Pavlidis, and T. L. Brock are with the Center for High-Frequency Microelectronics and Solid State Electronics Laboratory, Department of Electrical Engineering and Computer Science, The University of Michigan, Ann Arbor, MI 48109-2122.

P. R. Berger is with the Optoelectronic Device Research Department, AT&T Bell Laboratories, Murray Hill, NJ 07974.

IEEE Log Number 9143758.

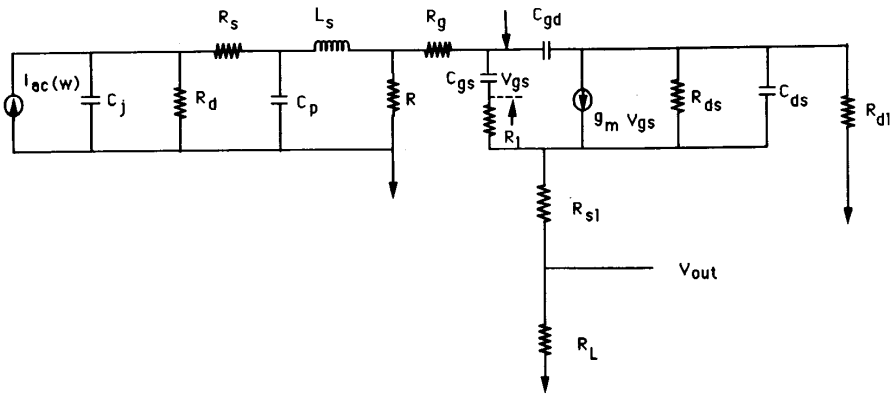

C_j = variable	R_d = 100MΩ	R_s = 20Ω	L_s = 0.6 nH
C_p = 10fF	R = 50Ω	R_g = 0.5Ω	R_{gs} = 10K
C_{gs} = 0.31pF	R_1 = 7.44Ω	R_{sl} = 3.5Ω	R_L = 50Ω
C_{gd} = 0.038 pF	C_{ds} = 0.11pF	R_{dl} = 23Ω	R_{ds} = 209Ω

Fig. 1. Equivalent circuit p-i-n FET photoreceiver.

a 0.3-μm GaAs FET integrated with an InGaAs p-i-n photodiode. These authors extended the bandwidth using a capacitor and/or inductor in the circuit. They call this a peaking technique, and it is shown in the next section that the addition of an inductive element does indeed extend the bandwidth.

Modulation-doped FET's and p-i-n photodiodes are both appropriate for low-noise receiver applications. Great strides have been made in the development of low-noise MODFET's with both GaAs- and InP-based systems for use at the microwave and millimeter-wave frequencies [12], [14]. In this paper we will describe and discuss our results on the performance characteristics of InP-based monolithically integrated p-i-n MODFET front-end photoreceivers realized by both one-step molecular beam epitaxy and by epitaxial regrowth and two-step epitaxy.

II. Design Considerations: Calculated Frequency Response

The design of an optical receiver is much more complicated than that of a transmitter because the receiver must first detect weak, distorted signals and then make decisions on what type of data were transmitted, based on the amplified signal. Here we are primarily interested in the design of the front-end of a photoreceiver which consists of the photodetector followed by a preamplifier. There are essentially three design approaches to a front-end receiver. The first is the low-impedance design, so called because the diode biasing resistance R has low value. The second one is the high-impedance design, because in this case R has a high value. The third one is the transimpedance approach, where a feedback resistance is used instead of the load resistance. It has been recently demonstrated that even a FET could be used as an active feedback element instead of a passive resistor [15]. The different configurations are useful for different applications. Our experimental work to be described here is based on the low-impedance design.

The most important parameters that determine the bandwidth of the receiver are the transit time of the generated carriers in the diode and the RC time constant of the circuit, which is shown in Fig.1. In this study, the analysis has been done in two steps. First, the frequency response of the p-i-n diode limited by transit time is calculated, using the following equation [16]:

$$J(\omega) = q\phi\alpha L\left[\frac{1 - e^{-\alpha L}}{\alpha L(\alpha L - i\omega t_n)} - \frac{e^{-\alpha L}(e^{i\omega t_n} - 1)}{i\omega t_n(\alpha L - i\omega t_n)}\right] - q\phi\alpha L\left[\frac{1 - e^{i\omega t_p}}{i\omega t_p(\alpha L + i\omega t_p)} - \frac{1 - e^{-\alpha L}}{\alpha L(\alpha L + i\omega t_p)}\right] \quad (1)$$

where ϕ is a constant depending on the incident optical power, α is the absorption coefficient in the i-region of the p-i-n diode, L is the depletion (absorption) length, ω is the frequency, and t_n and t_p are the electron and hole transit times, respectively.

The second step was to calculate the frequency response of the amplifier circuit including the diode capacitance and resistance. This has been done by using a SPICE program. The two are then combined to give the frequency response for the complete receiver. The effect of the parasitic capacitive and inductive elements in the receiver circuit were also examined. As the total capacitance increases, the $f_{3\,dB}$ frequency decreases, but the $f_{3\,dB}$

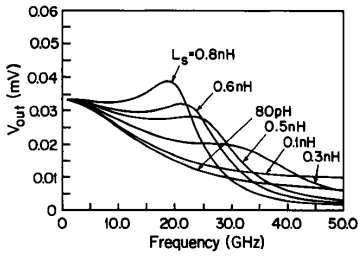

Fig. 2. Calculated frequency response of p-i-n FET integrated photoreceiver for different values of the series inductance L_s.

frequency will increase if a small inductance is added in series between the diode and the transistor. The calculated frequency response of the p-i-n FET circuit is shown in Fig. 2 for an i-region length of the diode of 1 μm and for different values of the coupling inductance. The other parameters used in the calculations are given alongside Fig. 1. We find that to improve the $f_{3\,dB}$ frequency response, the inductance value has to be properly chosen. This value is dependent on the value of the total capacitance and the biasing resistance in the circuit. The value of the biasing resistance should be small for high $f_{3\,dB}$ frequency. However, by making this resistance small, the gain of the amplifier and the S/N ratio will decrease, as we have found from a calculation of the noise figures, following Smith and Personick [17]. So, there is a tradeoff between the speed, the gain, and the noise performance as far as the proper value of the resistance is concerned. For high-gain applications, an enhancement in the transconductance would help.

III. Photoreceivers Realized by Vertical Integration

In this section we will describe the molecular beam epitaxial (MBE) growth, fabrication, and characteristics of InP-based $In_{0.53}Ga_{0.47}As$ p-i-n photodiodes vertically integrated with pseudomorphic $In_{0.6}Ga_{0.4}As/In_{0.52}Al_{0.48}As$ MODFET's to form a front-end photoreceiver. Pseudomorphic InP-based MODFET's have demonstrated high-frequency and low-noise performance which have surpassed that of their lattice-matched counterparts [14]. The enhanced performance characteristics largely result from a higher band offset in the conduction band and a larger Γ–L separation, and to a lesser extent due to reduced alloy scattering and electron effective mass [18].

A. Device Growth and Fabrication

The p-i-n MODFET photoreceiver structure, schematically shown in Fig. 3(a), was grown on semi-insulating InP substrate by single-step MBE. It consists of a p-i-n photodiode which has a 0.75 μm $In_{0.53}Ga_{0.47}As$ i-region sandwiched between p^+ and n^+ $In_{0.52}Al_{0.48}As$ layers, followed by a 1-μm undoped (high-resistivity) $In_{0.52}Al_{0.48}As$ layer for isolation and finally the $In_{0.6}Ga_{0.4}As/In_{0.52}Al_{0.48}As$ pseudomorphic single quantum well MODFET.

300 Å	n+	InGaAs	3E18	
200 Å	i	InAlAs		
40 Å	n +	InAlAs	5E18	
30 Å	i	InAlAs		
150 Å	i	$In_{0.6}Ga_{0.4}As$		
400 Å	i	InGaAs		
10Å/10Å	i	InGaAs/InAlAs	S.L.	20 periods
1 μm	i	InAlAs		
0.1 μm	n+	InGaAs	3E18	
0.3 μm	n+	InAlAs	3E18	
50 Å	i	InAlAs		
0.75 μm	i	InGaAs		
100 Å	i	InAlAs		
0.5 μm	p+	InGaAs	2E18	
0.5 μm	p+	InAlAs	2E18	
	S.I.	InP Substrate		

(a)

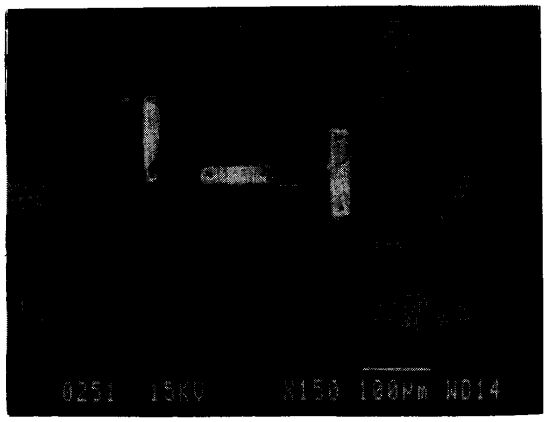

(b)

Fig. 3. (a) Schematic of heterostructure for p-i-n MODFET photoreceiver grown by molecular beam epitaxy. (b) Completed photoreceiver circuit with air-bridge connections.

The photoreceiver circuit shown in Fig. 4, was fabricated by a ten-level process. Different values of biasing resistance R were incorporated in the mask design to study their effect on the performance of the circuit. Monolithic inductors, as discussed in Section II, were also added and are seen in Fig. 3(b). The circuit was fabricated as follows: Ti(500 Å)/Au(500 Å) were first deposited for the purpose of alignment of the various levels. Next a 0.25-μm-deep mesa etch was done with $H_3PO_4 : H_2O_2 : H_2O$ for MODFET isolation, which stops at the isolating 1-μm $In_{0.52}Al_{0.48}As$ layer. A second mesa etch was done to reach the n^+ contact layer of the p-i-n diode. Ohmic contacts to the source and drain regions of the MODFET and the n^+

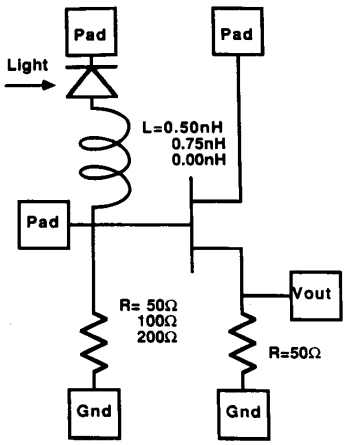

Fig. 4. p-i-n MODFET front-end photoreceiver circuit.

layer of the photodiode were made by electron-beam evaporation of Ge(700 Å)/Au(1400 Å)/Ni(500 Å)/Ti(200 Å)/Au(700 Å) and subsequent rapid thermal anneal for 10 s at 375°C in a nitrogen ambient. After appropriate gate recessing in the channel region Ti/Au were deposited to form gates of length 1 μm and width 200 μm. The source–drain separation is 3.5 μm. A third mesa was etched to reach the p^+ layer of the photodiode and ohmic contact to this layer was made by depositing Ti/Au. A fourth mesa was etched to reach the semi-insulating substrate for isolation of the devices. A 600-Å Ti film, which gives a sheet resistance of 15 $\Omega/\square$, was deposited for the delineation of the biasing and load resistances. Ti(0.1 μm)/Au(1.0 μm) were deposited to form interconnections and spiral inductors. Finally, appropriate processing steps were followed to form air bridges between the dual sources and other elements. This is seen clearly in the schematic of Fig. 3(b).

B. Performance Characteristics and Discussion

The measured dc current–voltage characteristics of 1-μm-gate MODFETs in the completed circuit show depletion mode behavior and good pinch-off characteristics. Typical measured dc current–voltage characteristics are shown in Fig. 5. The transistor corresponding to these data is characterized by I_{dss} = 460 mA/mm, G_{ds} = 50 mS/mm, and a pinch-off voltage of −0.5 V. The measured g_m of the MODFET in the completed circuit varied in the range 450–500 mS/mm.

The microwave performance of the MODFET's was determined from measured *S*-parameters in the frequency range 45 MHz to 18 GHz using a CASCADE wafer probing station. The cut-off frequency of the transistor has been evaluated by plotting the current gain as a function of frequency (Fig. 6) and is found to be 9 GHz. This result corresponds to the extrinsic performance of the device.

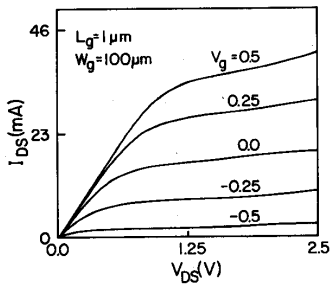

Fig. 5. Room-temperature drain current–voltage characteristics of 1-μm-gate $In_{0.6}Ga_{0.4}As/In_{0.52}Al_{0.68}As$ MODFET in photoreceiver circuit realized by vertical integration.

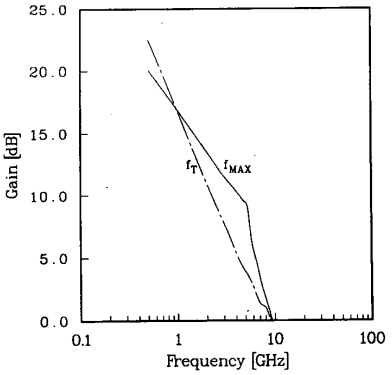

Fig. 6. High-frequency current gain and maximum available gain of pseudomorphic $In_{0.6}Ga_{0.4}As/In_{0.52}Al_{0.48}As$ MODFET.

The response speeds of the unconnected photodiodes of area 30 × 50 μm^2 and the p-i-n MODFET circuit were measured separately with a pulsed AlGaAs pulsed diode laser (λ = 850 nm) having a nominal pulsewidth of 100 ps. The photodiodes were mounted on a coplanar stripline and dc bias was provided through an HP 11612A bias-T network. The p-i-n MODFET was also similarly mounted for the response speed measurements. The microwave output resulting from pulsed photoexcitation was taken out from the drain or the source terminal through a second bias-T network. Best performance is oberved with the output signal from the source. The responsibility of the unconnected photodiode at ~4 V bias is ~0.65 A/W and the impulse response is characterized by a linewidth (FWHM) ~60 ps. The microwave output pulse response of the complete circuit to 100 ps laser excitation with the photodiode biased at 4 V is shown in Fig. 7. The rise time is limited by the laser pulse rise time. The FWHM is ~400 ps, which translates to a bandwidth of ~2 GHz. Circuits with different biasing resistance *R* and different coupling inductances were measured separately, and their temporal response characteristics are summarized in Table I. The data of Fig. 7 correspond to the circuit with *R* = 100 Ω and *L* = 0.5 nH.

The measured eye pattern for 1.7-Gb/s pseudorandom NRZ optical signals is shown in Fig. 8. If is seen that the

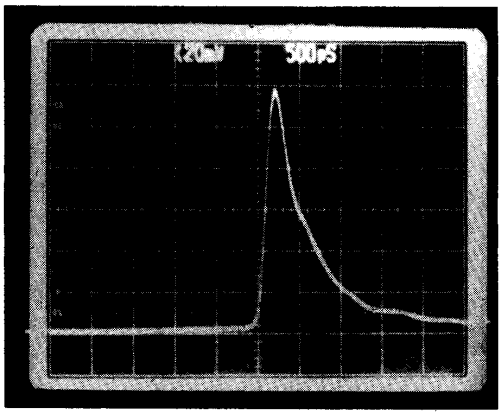

Fig. 7. Impulse response characteristics of monolithically integrated p-i-n MODFET front-end photoreceiver to 100-ps excitation.

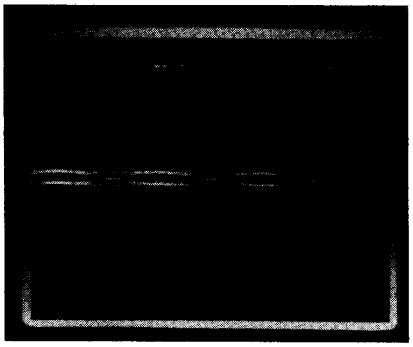

Fig. 8. Measured eye pattern of photoreceiver circuit for 1.7-Gb/s pseudorandom NRZ optical signal.

TABLE I
MEASURED p-i-n MODFET RESPONSE TIME TO 100-ps PULSED PHOTOEXCITATION FOR DIFFERENT VALUES OF BIASING RESISTANCE AND COUPLING INDUCTANCE

R (Ω)	L (nH)	FWHM (ps)
200	0.5	800
150	0.6	500
150	0	550
100	0.5	400

pattern (eye) is clearly open at this frequency. We are limited in experimental capability to test the circuit at higher bit rates, but believe that the circuit has a bandwidth higher than 2 GHz, as will be evident in the next section. However, this is one of the highest bandwidths achieved in an InP-based photoreceiver.

It is clear that although the vertical integration scheme with one-step epitaxy lends itself to easier realization of the photoreceiver circuit, the operational bandwidth falls short of the expected values. As mentioned earlier, in the vertical scheme of integration there exists a capacitive coupling under the electronic circuits due to the presence of the diode conducting layer. This parasitic capacitance degrades the microwave performance of the MODFET severely, as noted in the previous section. Due to this layer, there is a parasitic capacitance between the drain, the gate, and the source and the n^+ doped layer of the photodiode. Furthermore, the capacitance of the p-i-n diode adds to these parasitic capacitances. The equivalent circuit of the MODFET with the parasitic capacitances is shown in Fig. 9. From the measured S-parameters, the equivalent circuit element values were determined, and it was found that the parasitic capacitance added to the intrinsic capacitances of the MODFET. This gives a gate–source capacitance value 3–4 times larger than the intrinsic value, and a drain–gate capacitance value 15 times larger than the intrinsic value. This increase in the capacitance values is responsible for the degradation in the MODFET microwave performance. The values of the equivalent circuit elements were used in a SPICE simulation for the complete circuit and the calculated frequency response is shown in Fig. 10. The calculated 3-dB cutoff frequency is found to be 2.1 GHz which is in excellent agreement with the measured value derived from the impulse response measurements described in the previous section. To eliminate the parasitic capacitance, a proton implantation may be done under the contact areas of the MODFET in order to damage the material underneath constituting the diode. However, the dose and energy of such an implant needs to be very carefully controlled so that the MODFET channel properties are not degraded. We are in the process of exploring this possibility in order to improve the circuit bandwidth.

Some comments needs to be made about the discrepancy between the calculated bandwidths of Fig. 2 and that of Fig. 10, remembering that the latter agrees with the measured bandwidth of ~2 GHz. The value of the biasing resistance R is very critical in determining the bandwidth. While a value of 50 Ω was used for calculating the frequency responses shown in Fig. 2, the experimental circuit values of 100–200 Ω were used for the calculated data of Fig. 10. Also, a capacitance value of 0.05 pF was used initially, while the real device capacitances are nearly four times this value for 1-μm-gate devices. This, together with the parasitic capacitances discussed above, due to the isolating InAlAs layers, increase the total capacitance. The net effect of increased R and C_{total} is to reduce the bandwidth by an order of magnitude. Because of this, the effect of coupling inductance in the actual circuit is greatly reduced.

IV. PHOTORECEIVERS REALIZED BY EPITAXIAL REGROWTH

An alternative way to realize the photoreceiver circuit with the same devices is to use epitaxial regrowth and two-step epitaxy. An added advantage in this case is the associated planarity. The interface region generated by molecular beam epitaxial regrowth has been studied by us

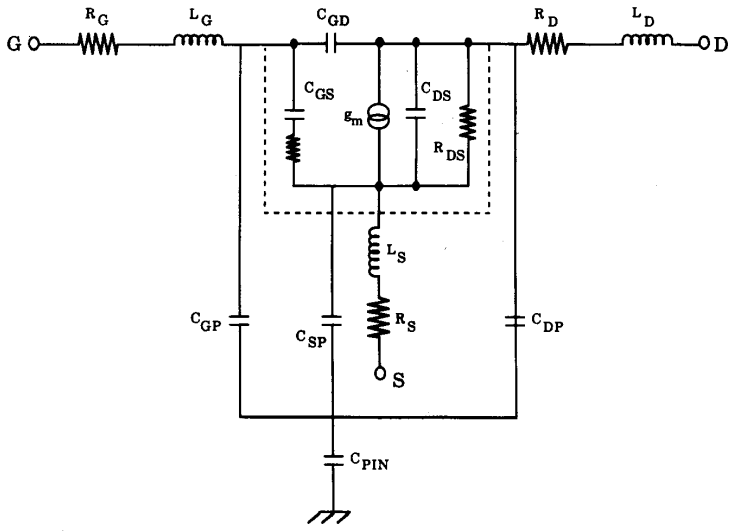

Fig. 9. Equivalent circuit of MODFET in photoreceiver circuit with parasitic capacitances.

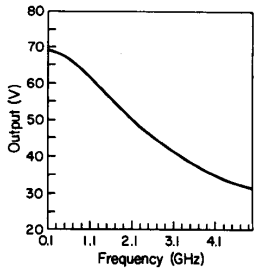

Fig. 10. Calculated frequency response p-i-n MODFET circuit taking into account the effect of parasitic elements.

[19] in detail. Combinations of wet chemical etching and dry etching (ion milling) with and without annealing were used to establish the best procedure for integrated technologies during regrowth.

In the context of the photoreceivers, it is of interest to measure the high-speed performance of regrown p-i-n photodiodes and MODFET's. We have investigated the temporal response characteristics of two types of regrown photodiodes. In the first with a total i-region thickness of 1.5 μm, the regrown interface is nearly in the middle of the i-region. After growth of the first step, the surface was ion-milled (0.3 μm) and lamp-annealed at 900°C for 7 s. The measured interface state density is $\sim 1 \times 10^{11}$ cm^{-2}. Gold Schottky diodes of area 25 μm^2 were defined by mesa etching. The temporal response characteristics were measured with 100-ps laser pulse excitation and a response time (FWHM) of 250 ps was obtained. For these diode dimensions an as-grown homojunction diode has a response time (FWHM) of $\sim$200 ps. In the second device, the entire p-i-n diode (with a 0.75-μm i-region) is regrown on the substrate after removal of the first epitaxial layer by etching with $1H_3PO_4 : 1H_2O_2 : 8H_2O$. The temporal response of 30 μm $\times$ 40 μm mesa-etched photodiodes to 100-ps intrinsic photoexcitation was an FWHM of $\sim$500 ps. It is therefore clear that interface states and/or deep levels created in the regrown layer degrade the high-frequency performance of regrown photodiodes. At the same time the dark current is higher. We have also compared the characteristics of as-grown and regrown $In_{0.53}Ga_{0.47}As/In_{0.52}Al_{0.48}As$ 1-μm-gate MODFET's lattice-matched in InP. Epitaxial regrowth of the MODFET was done on the substrate after selectively removing 2 μm of InGaAs grown in the first epitaxial step. In general, the normally grown devices showed larger transconductance and larger drain current values. Also, the output conductance was found to be higher in the regrown devices compared to the normally grown ones. The kink effect, where a negative resistance can be seen slightly past the knee voltage of I_{ds} versus V_{ds} characteristic, seemed to be more evident in the regrown devices than in the normally grown devices. It is generally believed that the kink in the transistor characteristics is due to trapping and detrapping in the buffer layer beneath the active channel. It has been shown recently [20] that by growing the InAlAs buffer at very low temperatures, in which the trapping/recombination times are made very short, the kink effect is greatly reduced. We believe that the density of slow traps are increased in the regrown InAlAs underneath the channel. Typically microwave characteristics for the normally grown and regrown MODFET's are shown in Fig. 11(a) and (b). The normally grown devices have a cutoff frequency f_{max} ranging from 45 to 55 GHz while the regrown devices have f_T ranging from 13 to 20 GHz and f_{max} ranging from 25 to 35 GHz. From the measured dc characteristics and the equivalent circuit obtained by fitting the measured S-parameters, it is evident that the main con-

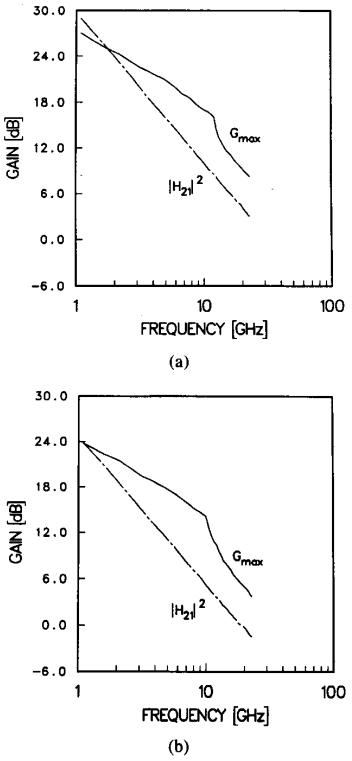

Fig. 11. Variation of current gain and maximum available gain with frequency for (a) normally grown, and (b) regrown MODFET with 1 × 100 μm^2 gate.

tributors to slightly inferior microwave performance in the regrown devices are larger source resistance, a larger output conductance, and a lower g_m value. In spite of these facts the regrown MODFET performance is promising for their integration with as-grown p-i-n photodiodes to form high-bandwidth photoreceivers. It is apparent that in the scheme of the photoreceiver circuit, a regrown MODFET will not degrade the bandwidth as much as a regrown photodiode.

A. Circuit Fabrication

p-i-n MODFET planar photoreceivers were realized using epitaxial regrowth. 1.0- and 0.25-μm gate-length pseudomorphic $In_xGa_{1-x}As/In_{0.52}Al_{0.48}As$ MODFET's were used for the circuits. The cross-sectional schematic of the integrated devices and an SEM photograph of the completed circuit with a 1.0-μm-gate MODFET are shown in Fig. 12(a) and (b). First, the p-i-n photodiode with a 1.0-μm $In_{0.53}Ga_{0.47}As$ absorption region sandwiched between p^+ and n^+ $In_{0.52}Al_{0.48}As$ layers was grown on a semi-insulating InP substrate. Then, SiO_2 was deposited on the layer using plasma-enhanced chemical vapor deposition (PECVD) and holes were etched to the InP substrate for epitaxial regrowth of the MODFET. A 150-Å $In_{0.60}Ga_{0.40}As$ channel was used for the pseudomorphic MODFET. After the regrowth of the MODFET, the SiO_2 layer and the polycrystalline material above it were selectively etched off. This leaves the MODFET and the p-i-n photodiode adjacent to each other. The p-i-n photodiode was first fabricated after defining the diode area using a wet chemical etch. Then, SiO_2 was deposited for passivation and antireflective coating. Openings were etched in the SiO_2 and then the top n^+ ohmic contact was formed using Ge/Au/Ni/Ti/Au. A second mesa etch was used to reach the p^+ contact layer and the bottom p^+ ohmic contact was formed using Zn/Ni/Au. For the MODFET, device mesa isolation was achieved by a 0.2–0.25-μm wet chemical etch. Then, the ohmic contacts were formed by evaporating Ge/Au/Ni/Ti/Au in the source and drain regions. The source-to-drain separation for the 1.0- and 0.25-μm-gate devices were 3.5 and 2.0 μm, respectively. The wafer was lamp annealed at 375°C for 10 s. Typical contact resistances were found to be approximately 0.2–0.3 $\Omega \cdot$ mm, measured by transmission line measurements, and the quality of metal after annealing showed good morphology and edge definition which is important especially for electron-beam lithography. For the 1.0-μm-gate devices, optical lithography was used while for the 0.25-μm-gate devices, electron-beam lithography using a single layer of PMMA was used. Prior to gate metal evaporation of Ti/Au, a gate recess was done using a citric acid wet etch until a predetermined source–drain current was achieved. Thin-film resistors were achieved by evaporating 600 Å of Ti. Then, very thick Ti/Au was evaporated for contact pads and interconnection. Finally, air bridges were formed to connect the two source pads on the MODFET and for connecting other elements.

B. Performance Characteristics

Room-temperature dc characterization was done on the regrown pseudomorphic $In_{0.70}Ga_{0.30}As/In_{0.52}Al_{0.48}As$ MODFET's. The 1.0-μm-gate device showed a peak transconductance of 300 mS/mm with a channel current of 200 mA/mm while the 0.25-μm-gate device showed a peak transconductance of 500 mS/mm with a channel current of 300 mA/mm. All the devices were biased at a drain voltage of 1.5 V. The p-i-n photodiode showed a dark current less than 10 nA at a bias of −10 V and a capacitance of 0.05 pF at a bias of −5 V. The p-i-n photodiode had an area of 630 μm^2. The scattering parameters were measured using an HP8510 automatic network analyzer and a CASCADE wafer probe station from 0.5 to 26.5 GHz at various gate and drain bias voltages. The 1.0-μm-gate device had an extrapolated current-gain cutoff frequency value f_T of 20 GHz and an extrapolated maximum available gain cutoff frequency f_{max} of 80 GHz while the 0.25-μm-gate device showed an f_T of 72 GHz and an f_{max} of 80 GHz (shown in Fig. 13). The circuit response speed was measured in a coplanar waveguide test fixture (DESIGN TECHNIQUES). DC bias was provided through HP 11612A bias tees. The microwave output was

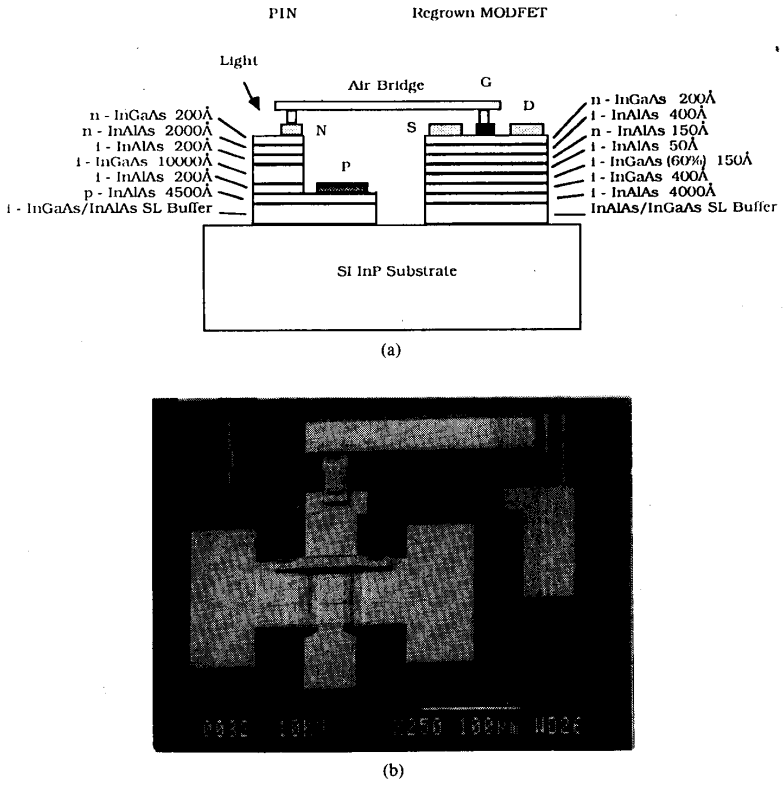

Fig. 12. InP-based front-end photoreceiver using regrowth. (a) Device schematic. (b) Photomicrograph of photoreceiver circuit.

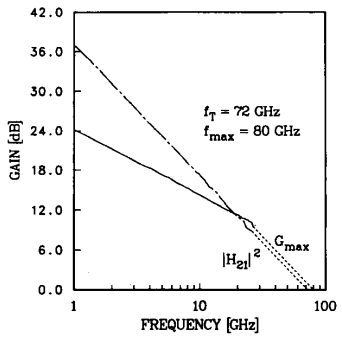

Fig. 13. High-frequency current gain and maximum available gain of regrown 0.25-μm-gate $In_{0.7}Ga_{0.3}As/In_{0.52}Al_{0.48}As$ MODFET in planar photoreceiver circuit.

taken from the drain terminal of the MODFET and into a sampling oscilloscope. A dye laser with a wavelength of 590 nm and a pulsewidth of 10 ps was used for photoexcitation of the p-i-n photodiode. For each circuit, the value of the biasing resistor R was 100 Ω while the gate widths of the MODFET's were 150 μm. The resulting output pulse response of the circuit with the p-i-n photodiode biased at -5 V and the drain terminal of the MODFET biased at 1.5 V are showed in Fig. 14(a) and (b). The FWHM for the circuit with the 1.0-μm-gate MODFET was 110 ps which translates to an estimated bandwidth of 4 GHz while the FWHM for the circuit with the 0.25-μm-gate MODFET was 60 ps which translates to a bandwidth of 6.5 GHz. The long tail observed in the output pulse response is believed to be caused by diffusion due to the fact that much of the light is absorbed in the top $In_{0.52}Al_{0.48}As$ layer. To our knowledge these are among the best measured values in integrated photoreceivers, approaching those measured in the best hybrid circuits.

V. Conclusions

In conclusion, we have analyzed and calculated the frequency response of a monolithically integrated front-end photoreceiver consisting of a p-i-n photodiode and a MODFET amplifier. We have experimentally investigated the performance characteristics of an InP-based photoreceiver in which the p-i-n diode and the MODFET are integrated in two different ways. The first is a vertical scheme using one-step molecular beam epitaxy It is seen that the microwave performance of the 1-μm-gate MODFET is degraded due to additional parasitic capacitances formed between the channel and the conducting layers of the p-i-n diode, with the isolating InAlAs layer acting as the dielectric. In spite of this limitation, the circuit bandwidth is >2 GHz. The second scheme of integration of

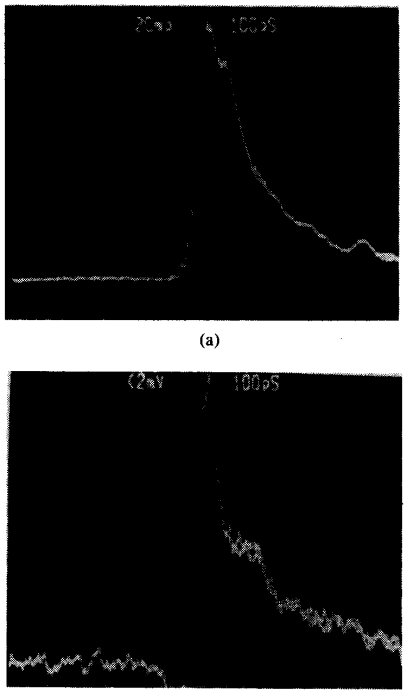

Fig. 14. Impulse response characteristics of planar p-i-n MODFET photoreceiver with (a) 1-μm-gate MODFET and (b) 0.25-μm-gate MODFET to 10-ps pulse excitation at 590 nm on photodiode.

these devices is a planar one and involves regrowth. Preliminary work done by us shows that the performance characteristics of regrown InP-based MODFET's are not severely degraded in terms of microwave performance, whereas those of the p-i-n diode are. We have therefore integrated high-speed photodiodes with 1- and 0.25-μm-gate MODFET's and the measured temporal response of the circuits indicates a bandwidth of 4–6.5 GHz depending on MODFET gate length.

Acknowledgment

The authors wish to thank J. Pamulapati for molecular beam epitaxial growth, M. Tutt for help in microwave measurements, and J. Harrang for the eye diagram measurements. Useful discussions with S. Ray and W-Q. Li are gratefully acknowledged.

References

[1] S. Miura, O. Wada, and K. Nakai, "A novel planarization technique for optoelectronic integrated circuits and its application to a monolithic AlGaAs/GaAs PIN-FET," *IEEE Trans. Electron. Devices*, vol. ED-34, p. 241, 1987.

[2] O. Wada, H. Hamaguchi, S. Miura, M. Makiuchi, K. Nakai, H. Horimatsu, and T. Sakurai, "AlGaAs/GaAs PIN photodiode/preamplifier monolithic photoreceiver integrated on a semi-insulating GaAs substrate," *Appl. Phys. Lett.*, vol. 46, p. 981, 1985.

[3] S. Miura, O. Wada, M. Makiuchi, and K. Nakai, "Optoelectronic integrated AlGaAs/GaAs p-i-n/field-effect transistor with an embedded, planar p-i-n photodiode," *Appl. Phys. Lett.*, vol. 48, p. 1461, 1986.

[4] D. Wake, E. G. Scott, and I. D. Henning, "Monolithically integrated InGaAs/InP PIN-FET photoreceiver," *Electron. Lett.*, vol. 22, p. 719, 1986.

[5] O. Wada, T. Sakurai, and T. Nakagami, "Recent progress in optoelectronic integrated circuits," *IEEE J. Quantum Electron.*, vol. QE-21, p. 805, 1986.

[6] S. J. Kim, G. Guth, G. P. Vella-Coleiro, C. W. Seabury, W. A. Sponsler, and B. J. Rhoades, "Monolithic integration of InGaAs p-i-n photodetector with fully ion-implanted InP JFET amplifier," *IEEE Electron Devices Lett.*, vol. 9, p. 447, 1988.

[7] J. C. Renaud, L. Nguyen, M. Allovon, F. Heliot, F. Lugiez, and A. Scavennec, "Monolithic photoreceiver integrating GaInAs PIN/JFET with diffused junctions," *Electron. Lett.*, vol. 23, p. 1055, 1987.

[8] K. Kasahara, J. Hayashi, K. Makita, K. Taghuchi, A. Suzuki, H. Nomura, and S. Matushita, "Monolithically integrated InGaAs PIN/InP MISFET photoreceiver," *Electron. Lett.*, vol. 20, p. 314, 1984.

[9] K. Matsuda, M. Kubo, K. Ohnaka, and J. Shibata, "A monolithically integrated InGaAs/InP photoreceiver operating with a single 5-V power supply," *IEEE Trans. Electron. Devices*, vol. 35, p. 1284, 1988.

[10] H. Nobuhara, H. Hamaguchi, T. Fujii, O. Aoki, M. Makiuchi, and O. Wada, "Monolithic PIN-HEMT receiver for long wavelength optical communication," *Electron. Lett.*, vol. 24, p. 1246, 1988.

[11] Y. Miyagawa, Y. Miyamoto, and K. Hagimoto, "7 GHz bandwidth optical front-end circuit using GaAs FET monolithic IC technology," *Electron. Lett.*, vol. 25, p. 1306, 1989.

[12] P. C. Chao *et al.*, "94 GHz low-noise HEMT," *Electron. Lett.*, vol. 25, p. 504, 1989.

[13] U. K. Mishra, A. S. Brown, and S. E. Rosenbaum, "DC and RF Performance of 0.1 μm gate length $Al_{0.48}In_{0.52}As$-$Ga_{0.38}In_{0.62}As$ pseudomorphic HEMTs," in *IEDM Tech. Dig.*, p. 180, 1988.

[14] P. C. Chao, A. J. Tessmer, K-H. G. Duh, P. Ho, M-Y. Kao, P. M. Smith, J. M. Ballingall, S-M. J. Liu, and A. A. Jabra, "W-band low-noise InAlAs/InGaAs lattice-matched HEMTs," *IEEE Electron. Device Lett.*, vol. 11, p. 59, 1990.

[15] J. J. Brown, D. C. W. Lo, J. T. Gardner, Y. K. Chung, C. D. Lee, and S. R. Forrest, "$In_{0.53}Ga_{0.47}As$ junction field-effect transistors as tunable feedback resistors for integrated receiver preamplifiers," *IEEE Electron Device Lett.*, vol. 10, p. 588, 1989.

[16] Y. Zebda, Ph.D. dissertation, University of Michigan, Ann Arbor, 1989.

[17] R. G. Smith and S. D. Personick, "Receiver design for optical fiber communication system," in *Semiconductor Devices for Optical Communication*. New York, NY: Springer-Verlag, 1980, ch. 4.

[18] W-P. Hong, G. I. Ng, P. K. Bhattacharya, D. Pavlidis, and S. Willing, "Low- and high-field transport properties of pseudomorphic $In_xGa_{1-x}As/In_{0.52}Al_{0.48}As$ ($0.53 \leq x \leq 0.65$) modulation doped heterostructures," *J. Appl. Phys.*, vol. 64, p. 1945, 1988.

[19] D. Biswas, P. R. Berger, U. Das, J. E. Oh, and P. K. Bhattacharya, "Investigation of the interface region produced by molecular beam epitaxial regrowth," *J. Electron. Mater.*, vol. 18, p. 137, 1989.

[20] A. S. Brown, U. K. Mishra, C. S. Chou, C. E. Hooper, M. A. Melendes, M. Thompson, L. E. Larson, S. E. Rosembaum, and M. J. Delaney, "AlInAs-GaInAs HEMT's utilizing low-temperature AlInAs buffers grown by MBE," *IEEE Electron. Device Lett.*, vol. 10, p. 565, 1989.

*

Yousef Zebda received the B.S. degree in electrical engineering in Jordan and the M.S. and Ph.D. degrees from the University of Michigan, Ann Arbor, in 1987 and 1989, respectively. His doctoral research was based on studies of monolithically integrated electronic and optoelectronic devices.

Currently he is Assistant Professor at Jordan University of Science and Technology at Irbid, Jordan.

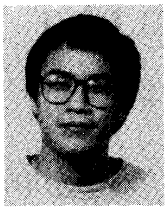

Richard Lai received the B.S. degree in electrical engineering at the University of Illinois, Urbana, in 1986 and the M.S.E.E. degree from the University of Michigan, Ann Arbor, in 1988.

Currently he is working towards the Ph.D. degree in electrical engineering at the University of Michigan. His research involves studying InP-based MODFET's for applications in InP-based MMIC and OEIC circuits.

*

Pallab Bhattacharya (M'78-SM'83-F'89) received the B.Sc. degree with honors in physics in 1968, and the B.Tech. and M.Tech. degrees in radio physics and electronics in 1970 and 1971, respectively, all from the University of Calcutta, India. He received the M.Eng. and Ph.D. degrees in 1976 and 1978, respectively, from the University of Sheffield, England.

From 1975 to 1978, he was with the Electronics and Electrical Engineering Department, University of Sheffield, where his doctoral research dealt with the investigation of deep-level defects in GaAs and (Al,Ga)As. From 1978 to 1983, he was a member of the Electrical Engineering faculty at Oregon State University, Corvallis, where he established facilities for epitaxial growth and characterization of III-V semiconductors. There he worked on phase equilibria and LPE growth of high-purity InGaAs and InGaAsP, their low- and high-field transport properties and detailed electrical and optical characterization of MOCVD-grown AlGaAs. He also demonstrated extremely low noise performance in InGaAs:Fe photoconductive detectors. He spent the 1981-1982 academic year as an Invited Professor of the Swiss Federal Institute of Technology, Lausanne, where he worked on molecular beam epitaxy and the fabrication of high-speed detectors. He is currently Professor of Electrical Engineering and Computer Science at the University of Michigan, Ann Arbor, and Director of the Solid-State Electronics Laboratory. His research interests include LPE and MBE growth of III-V semiconductors and their electrical and optical properties, photodetectors, quantum well devices, and integrated-optical devices.

Dr. Bhattacharya is a member of the American Physical Society and Sigma Xi. He received the Alexander von Humboldt Award in 1980.

*

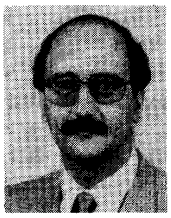

Dimitris Pavlidis (S'73-M'76-SM'83) received the B.Sc. degree in physics from the University of Patras, Greece, in 1972, and the Ph.D. degree from the University of Newcastle, Newcastle-upon-Tyne, England, in 1976. He continued as Postdoctoral Fellow at Newcastle until 1978, engaged in work on microwave semiconductor devices and circuits.

In 1978 he joined the High Frequency Institute of the Technical University of Darmstadt, Germany, working on III-V devices and establishing a new semiconductor technology facility. In 1980 he worked at the Central Electronic Engineering Research Institute, Pilani, India, as UNESCO consultant. During 1980-1985 he was Engineer and Manager of the GaAs Monolithic Microwave Integrated Circuits (MMIC) Group of Thomson-CSF, Corbeville, France. In this capacity he was responsible for projects on monolithic power and broad-band amplifiers, tunable oscillators, optical preamplifiers, phase shifters, attenuators, their technology and process evaluation, and the establishment of a component library for MMIC applications. He has been Professor of Electrical Engineering and Computer Science at the University of Michigan, Ann Arbor, since 1986. His current research interests cover the design and fabrication of HEMT's, HBT's, and III-V microwave and millimeter-wave devices and monolithic heterostructure IC's. His publications are in microwave semiconductor devices and circuits and he holds six patents on MMIC applications. In 1990 he was awarded the European Microwave Prize for his work on InP-based monolithic integrated HEMT amplifiers.

*

Paul R. Berger (S'84-M'91) received the B.S.E. degree in engineering physics in 1985, and the M.S.E. and Ph.D. degrees in electrical engineering in 1987 and 1990, respectively, all from the University of Michigan, Ann Arbor. His Ph.D. dissertation studied MBE growth kinetics of strained III-V semiconductors using RHEED, MBE selective area regrowth, and the application of these to monolithically integrated optoelectronics including guided-wave detectors/modulators and photoreceivers.

Since August 1990 he has been employed as a postdoctorate at AT&T Bell Laboratories, Murray Hill, NJ, in the Optoelectronic Device Research Department. His current research interests include semiconductor lasers and monolithic integration of optoelectronic devices.

Dr. Berger is a member of the Optical Society of America.

*

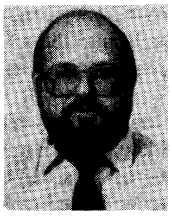

Timothy L. Brock has been a Research Engineer at the University of Michigan, Ann Arbor, since October 1989. His primary responsibilities involve electron beam lithography relating to submicrometer circuit and device fabrication. Prior to this he held a research position at the University of Illinois, Urbana, and has been involved with several publications involving electron beam applications.